J. Coat. Technol. Res., **20** (1) 73–86, 2023
https://doi.org/10.1007/s11998-022-00710-1

Challenges of fabricating catalyst layers for PEM fuel cells using flatbed screen printing

Linda Ney, Jakob Hog, Rajveer Singh, Nathalie Göttlicher, Patrick Schneider, Sebastian Tepner, Matthias Klingele, Roman Keding, Florian Clement, Ulf Groos

Received: 6 February 2022 / Revised: 30 August 2022 / Accepted: 5 September 2022
© The Author(s) 2022

Abstract In this work, flatbed screen printing is evaluated regarding its capability to produce catalyst layers of PEM fuel cells. In the field of printed electronics, screen printing is regarded as robust and high-throughput coating technology. The possibility of in-plane structuring could be an additional degree of freedom, enabling more complex designs of catalyst layers in the future. In this study, process parameters are varied to investigate their effect on resulting layer thickness, homogeneity, and Pt-loading. With the usage of different screens, the Pt-loading can be adjusted. Additionally, two different pastes with and without water content are investigated. The catalyst paste without water showed a better process stability during printing and performed best under dry conditions (RH = 40%) and worst under wet conditions (RH = 100%) during electrochemical in-situ testing. Overall, the reproducibility of the CCM production process was verified. The viscosity of the catalyst paste with 19.55 wt% water in solvent was higher compared to the paste without water. Furthermore, a carbon paste (Pt-free) is developed in a similar viscosity range as the catalyst pastes. The main challenge of screen printing process development lies in the paste optimization to prevent evaporation effects over time, ensuring sufficient wetting of the paste on the substrate and sufficient fuel cell performance.

This paper was presented at the 14th European Coatings Symposium held in 2021 in Brussels, Belgium.

L. Ney (✉), J. Hog, R. Singh, N. Göttlicher, P. Schneider, S. Tepner, M. Klingele, R. Keding, F. Clement, U. Groos
Fraunhofer Institute for Solar Energy Systems, Freiburg, Germany
e-mail: linda.ney@ise.fraunhofer.de

Keywords Catalyst layer, Fuel cell, Screen printing, Catalyst ink, Solvent evaporation

Introduction

Today's fuel cell catalyst production research addresses the challenges of upscaling and optimizing various fabrication processes, in order to increase throughput rates while maintaining quality demands.[1,2] Different routes of fabrication are possible: The catalyst paste can be applied directly onto the membrane[3,4] or gas diffusion layer[5,6] or indirectly by using the decal transfer method.[7,8] In general, the catalyst suspensions consist of platinum on carbon powder, ionomer dispersion and a mixture of solvents. Depending on the preferred coating technology the solid content of the suspension can vary. After coating, the wet layers are dried and later transferred, which can be seen in Fig. 1. Often catalyst layers are produced by spray coating,[6,9,10] electrospinning,[11–13] inkjet printing[14,15] or blade coating.[15–17] However, the transformation from laboratory to industrial scale requires the evaluation of high-throughput coating technologies. Besides slot die coating, gravure or flexographic printing, the screen printing process has demonstrated a very good reliability, homogeneity of the printed layers and suitability for high throughput, coming from fields like printed electronics and graphic printing[7].

The screen printing process can be divided in two steps. During the first step (''flooding''), the paste is spread over the screen filling the mesh. Secondly (''printing''), the printing squeegee pushes the screen down, so that it slightly touches the substrate. The movement of the squeegee pushes the paste through the screen where it is separated dependent on the snap-off distance and squeegee speed.[18,19]

The filament breakup underneath the screen has been studied in-depth by Potts et al.[18] This effect is not

only dependent on the process parameters, but also on the surface energies of the paste, substrate, screen and many more as can be seen in Fig. 2. For example, higher squeegee speeds result in higher deposition weights, which is additionally dependent on paste viscosity. Lower viscosity pastes could be printed with higher squeegee speeds. However, Riemer[20] states that exceeding a defined squeegee speed negatively affects printing results.

In this study, flatbed screen printing is applied by using a semi-automatic screen printer, which enables process control, sufficiently high layer thicknesses and the potential of high throughput. In contrast to slot-die coating, screen printing enables the manufacturing of in-plane structures of catalyst layers. In this work, printing process parameters are varied to investigate their effect on the printed layers. Therefore, a less expensive platinum-free paste (carbon paste) with similar viscosity like the catalyst suspensions is produced. Finally, the influence of water content in catalyst suspensions is investigated regarding the screen printing process stability and electrochemical in-situ performance of the fuel cells.

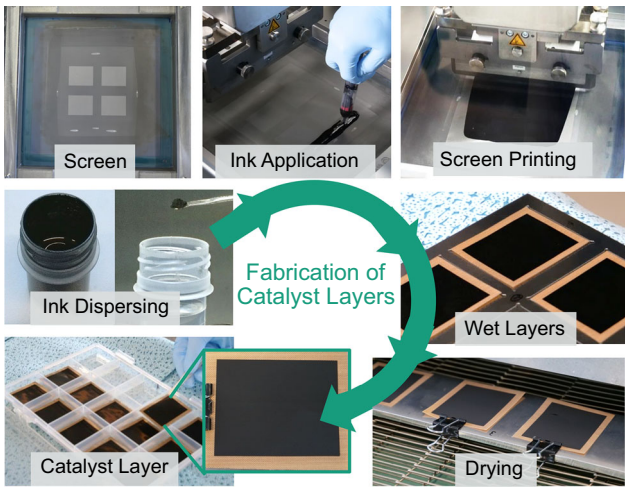

Fig. 1: Process route of fabricating catalyst layers by screen printing at Fraunhofer ISE

Experimental methods and materials

Catalyst suspension

To produce the platinum-free carbon paste, Vulcan XC72R carbon black powder (Cabot Corp.), ionomer dispersion (Aquivion D79-25BS, 25 wt% in water) and a mixture of (5:6) PGME (propylene glycol methyl ether) and EG (ethylene glycol) is homogenized by magnetic stirring and rotation of a dual axisymmetric centrifuge (SpeedMixer, Hauschild GmbH & Co. KG). The water content of the ionomer dispersion has been evaporated prior to adding the carbon powder,[24] which resulted in a paste solid content of 18 wt% with an ionomer-to-carbon ratio of 0.7.[8]

The functional catalyst suspensions (with platinum) have been made of Umicore Elyst Pt50 0550 powder (50 wt% Pt on HSC) for cathode side and Umicore Elyst Pt20 0390 powder (20 wt% Pt on LSC) for anode side. The ionomer type, including I/C ratio, and solvents are kept the same as mentioned above. Additionally, two different cathode water contents

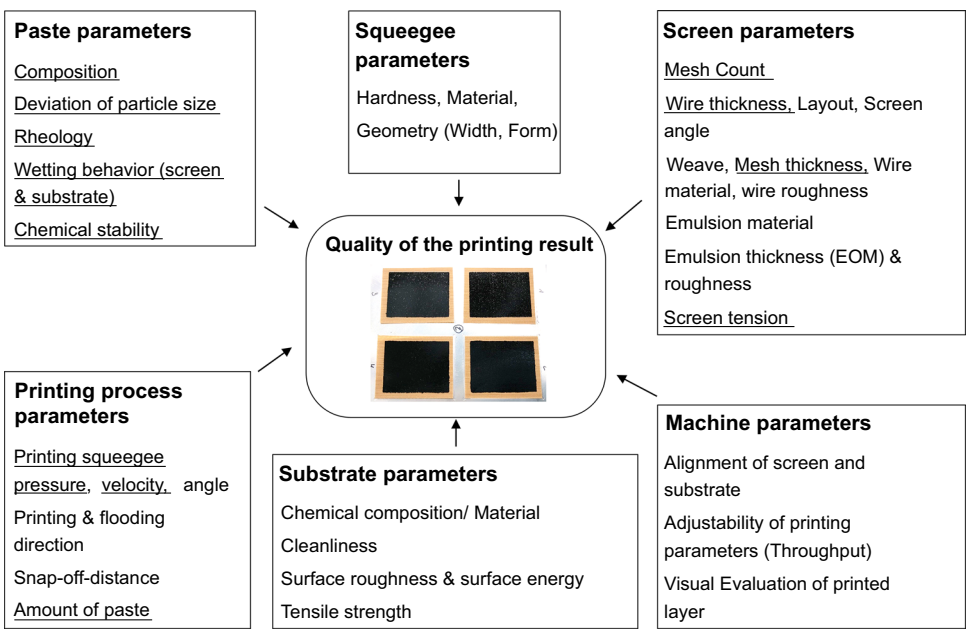

Fig. 2: Overview on screen printing process parameters that affect the quality of printed structures.[20–23] All underlined parameters are varied in this study

Table 1: Characteristic properties of different suspensions prepared and printed in this study

Suspension name	Pt on carbon (wt%)	I/C (–)	Solid content (wt%)	Water in solvent content (wt%)	Carbon-to-solvent ratio (–)
Carbon paste	0	0.70	17.91	0	0.128
Cathode paste without water	47.03	0.71	19.33	0	0.092
Cathode paste with water	47.03	0.70	19.37	19.55	0.093
Anode paste	19.46	0.71	25.02	17.20	0.172

The Pt/C ratio is taken from catalyst manufacturer information. All other values are measured during paste production by weighing.

have been prepared: 0 wt% and 19.55 wt% water within the liquid part. Table 1 summarizes the specifics of each suspension.

Rheological characterization

A rotational rheometer with Twin Drive© technique (MCR702 Twin Drive, Anton Paar) has been used with simultaneous rotation of upper and lower plate. The parallel plates with diameter of 50 mm and a gap height of 200 µm are rotated in opposite directions at a constant temperature of 20°C and have a roughened surface to reduce wall slip phenomena at low shear rates.[19,25,26] The pastes rested for 10 min before measurement. During the rotational measurement, the shear rate is logarithmically increased from $\dot{\gamma} = 0.1 - 3000\ \mathrm{s}^{-1}$ to measure the apparent viscosity η.[19,26] The static yield stress τ_y is determined by a logarithmic increase of shear stress during rotation from $\tau = 0.1 - 1000$ Pa. Additionally, oscillatory measurements are conducted to investigate the dynamic yield stress by varying the strain amplitude between $\gamma = 0.01$–1000% at a constant angular frequency of $\omega = 10$ rad/s. Each rheological measurement is repeated three times.

Flatbed screen printing process

All coatings are conducted with a semiautomatic flatbed screen printer (EKRA XH STS, ASYS Group) and screens bought from KOENEN GmbH. Different process parameters like type of mesh, printing squeegee velocity and squeegee pressure are varied systematically. The detailed ranges and combinations are shown in Fig. 3. Within this variation, a constant amount of the carbon paste (7.43 ± 0.13 g) is applied on the respective screen. Afterwards, as many layers as possible are printed, in which four coatings are printed simultaneously with a screen aperture of $A_{\mathrm{CL}} = 20\ \mathrm{cm}^2$ each (Fig. 1). The following parameters have been kept constant: snap-off distance $a = 1.8$ mm, separation distance $a_{\mathrm{s}} = 2$ mm, separation speed $v_{\mathrm{s}} = 2$ mm/s, flooding speed $v_{\mathrm{f}} = 80$ mm/s and printing squeegee angle $\alpha = 55°$. The squeegee area touching the screen could be estimated as $A_{\mathrm{sq}} = 1 \times 180$ mm. Therefore, the squeegee force of 50, 75 and 100 N can be transformed to pressure.

Three different screens are fabricated with stainless steel meshes, which thicknesses t are twice the wire diameter d, as can be seen from manufacturer information in Table 2 and illustrated in Fig. 4. In case of often used calendered meshes, the thickness would be less than twice the wire diameter. The commonly described mesh parameters refer to mesh count, wire diameter d and screen angle φ, as in "400/18/22.5" (MC / d /φ). The screen tension $\sigma_{\max}$ depends on the properties of the wire material (usually stainless steel) and geometry of the mesh.[23,27]

To calculate the theoretical volume of printed paste, some considerations within the cross-sectional geometry of the mesh must be made. The mesh can be divided in open parts, which will be filled by paste and closed parts of the wires. Therefore, the diagonal wire length within one mesh unit l, is calculated by equation (1).[28]

$$l = \sqrt{\left(\frac{1}{\mathrm{MC}}\right)^2 + \left(\frac{t}{2}\right)^2} \tag{1}$$

Horvath et al.[28] calculated the theoretical volume fraction of the wire within the mesh before calendering. In this study, we extend his equations to account for a possible reduced mesh thickness after calendering. The theoretical paste volume $V_{\mathrm{th,wet}}$ results from the subtraction of the wire volume V_{wire} from one entire mesh unit V_{MU} with the mesh thickness t. By multiplying with the mesh count MC, the resulting volume is normalized to the printed area, which equals the screen opening A_{CL}.

$$\begin{aligned} V_{\mathrm{th,wet}} &= (V_{\mathrm{MU}} - 2V_{\mathrm{wire}})\mathrm{MC}^2 \\ &= t - \pi\frac{\mathrm{d}^2}{2} l \cdot \mathrm{MC}^2 (\mathrm{mm}^3/\mathrm{cm}^2) \end{aligned} \tag{2}$$

However, the theoretical volume is an ideal geometrical value. The real deposited volume can differ due to adhesion-forces of the paste and the wires

<table>
<tr><th colspan="3">Group 1: Mesh variation</th><th colspan="4">Group 2: Printing speed variation</th><th colspan="3">Group 3: Pressure variation</th></tr>
<tr><td colspan="10">Carbon paste dispersing and homogenizing</td></tr>
<tr><td colspan="3">Squeegee pressure p = 417 kPa</td><td colspan="4">230/30 mesh</td><td colspan="3">Printing speed: v =100 mm/s</td></tr>
<tr><td>400/18 mesh</td><td>230/30 mesh</td><td>280/25 mesh</td><td>v = 50 mm/s</td><td>v = 100 mm/s</td><td>v = 200 mm/s</td><td>v = 300 mm/s</td><td>p = 278 kPa</td><td>p = 417 kPa</td><td>p = 556 kPa</td></tr>
<tr><td colspan="3">v = 100 mm/s</td><td colspan="4">Squeegee pressure p = 417 kPa</td><td colspan="3">230/30 mesh</td></tr>
<tr><td colspan="10">Drying at 110°C, 15 min</td></tr>
<tr><td colspan="10">Weighing of each (dry) layer</td></tr>
<tr><td colspan="10">Thickness measurement by SEM</td></tr>
</table>

Fig. 3: Design of experiment with variation of the process parameters mesh type, squeegee pressure and velocity for carbon paste (Pt-free)

Table 2: Manufacturer information about specific properties of the different screens used in this study

Screen type	Mesh thickness t (μm)	Mesh count MC (1/inch)	Wire diameter d (μm)	Specific theoretical wet volume $V_{th,wet}$ (mm^3/cm^2)	Specific wire surface of mesh $A_{surf,wire}$ (mm^2/cm^2)
400/18/22,5	36	400	18	2.8	185.1
280/25/22,5	50	280	25	3.9	179.6
230/30/22,5	60	230	30	4.7	176.9

Carbon paste density has been measured as ρ_{wet}= 1.082 ± 0.025 g/cm^3. $V_{th,wet}$ and $A_{surf,wire}$ are calculated with equations (2) and (4).

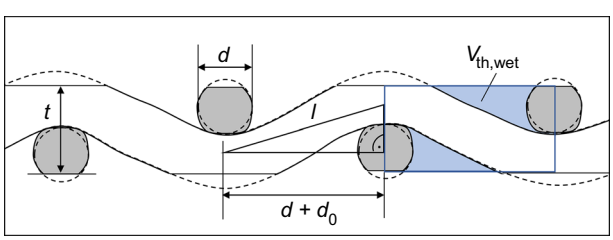

Fig. 4: Schematic representation of mesh cross section. The dashed line shows the mesh before calendering, solid line after calendering

within the screen. Additionally, many other process parameters (see Fig. 2) could lead to a significant change in mass transfer. If the paste composition is known (solid content χ_{solid} and paste density ρ_{wet}) and the printed layers are weighed $m_{CL,dry}$ after drying, the real applied volume of paste $V_{real,wet}$ can be estimated. This value is only valid if one does not consider any evaporation of solvents during the printing process.

$$V_{real,wet} = \frac{m_{CL,dry}}{\chi_{solid}\rho_{wet}A_{CL}}(\mathrm{mm}^3/\mathrm{cm}^2) \quad (3)$$

The second relevant mesh parameter might be the specific wire surface of each mesh type $A_{surf,wire}$. It can be calculated with equation (4).

$$A_{surf,wire} = \pi t l \mathrm{MC}^2(\mathrm{mm}^2/\mathrm{cm}^2) \quad (4)$$

If it was printed with functional catalyst paste, the Pt-loading ω_{Pt} can be recalculated by weighing the catalyst layer $m_{CL,dry}$, knowing the printed area A_{CL} and the platinum to solid content of the paste recipe $\chi_{Pt/solid}$, according to equation (5):

$$\omega_{Pt} = \frac{m_{CL,dry}}{A_{CL}}\chi_{Pt/solid} \quad (5)$$

Layer thickness measurement (SEM)

Each 9th print contains one silicon wafer as substrate. Due to their excellent cracking behavior and electrical conductivity, SEM cross sections are taken at four different points per substrate, resulting in eight pictures per process variation. An image processing tool has been developed to extract corresponding height data for each vertical pixel column of each SEM image to calculate the average layer thickness and its deviation.

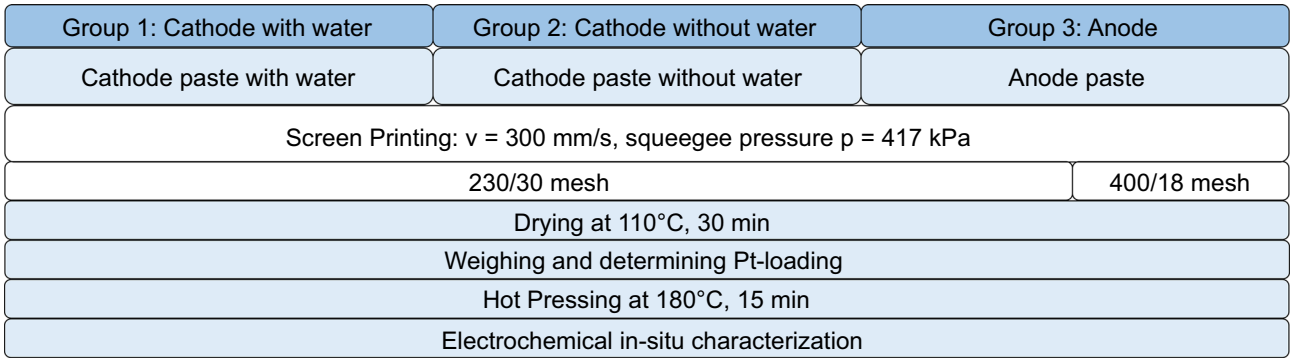

Fig. 5: Design of experiment to fabricate functional CCMs. Variation of water content on cathode side and layer weight on anode side by different meshes

MEA fabrication and electrochemical in-situ testing

At the end, functional catalyst pastes for anode and cathode (Table 1) were printed to verify the platinum-loading range at the anode and cathode side and investigate the effect of water as the solvent on the screen printing process. Two different screens have been used for coating the anode catalyst layers to analyze the impact on Pt-loading and hence fuel cell performance (Fig. 5).

Finally, the produced catalyst layers are transferred onto the membrane (Gore M735.18, 18 μm thickness) by hot-pressing at 180°C and 5 MPa pressure for 15 min (active area of 12 cm^2) and tested electrochemically to verify the fabrication route and their reproducibility. Due to higher thermal stability and increased glass transition temperature of Aquivion (short side chain ionomer), the hot-pressing temperature is higher than for Nafion.[8,29,30] Commercial gas diffusion layers Freudenberg H23C9 are used on both electrodes. For the in-situ performance characterization, UI-curves were measured under H_2/air conditions at 80°C with a Baltic FuelCells liquid cooling quickConnect® high amp test cell.[8] During the measurements a constant cell compression of 1.35 MPa and a volumetric flow rate of 2.0 slpm hydrogen at the anode and 5.0 slpm air at the cathode is applied. The polarization curves are taken in potentiostatic steps from open circuit voltage to 0.2 V at 100% RH and 2.0 bara gas pressure, and under dry conditions at 40% RH and 1.5 bara gas pressure. Each operating point is conditioned until a stationary cell current has been reached.

Results and discussion

Rheological characterization

The microstructure of catalyst pastes strongly influences the microstructure of the dry catalyst layer such as ionomer distribution, pore network or Pt/C agglomerate distributions and therefore effects the electrochemical performance of the fuel cell. These microstructure properties and changes are visible during rheological measurements of the catalyst paste. However, often different mechanisms and effects overlap and work concurrently.

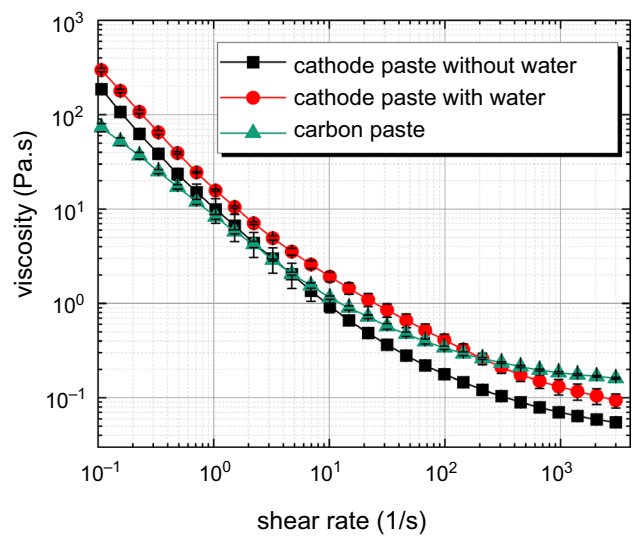

Fig. 6: Dynamic viscosity curves with increasing shear rate for different pastes (carbon and cathode pastes), showing strong shear thinning behavior

The shear-thinning behavior of carbon pastes is well known in the literature [17,31–35] and is advantageous during screen printing.[36] Increasing the shear rate, breaks up the microstructural cluster of the suspension, hence the dynamic viscosity decreases. Figure 6 shows the strong shear-thinning behavior within the power-law region, whereas at higher shear rates the infinity shear viscosity will be reached eventually. During the printing process, the apparent shear rate [equation (6)] can be estimated as the ratio of process speed (squeegee velocity) v and mesh opening d_0, which can be calculated from mesh count and wire diameter.[27,37]

$$\dot{\gamma} \approx \frac{v}{d_0} \tag{6}$$

Therefore, assuming a squeegee velocity of 300 mm/s and 400/18 mesh, the maximum apparent shear rate within this study would be estimated as $\dot{\gamma} \approx 6593\ s^{-1}$. The minimum appearing process shear rate would be $\dot{\gamma} \approx 622\ s^{-1}$. However, high shear rates cannot be measured easily due to spillage and edge fracture issues at the gap of the parallel plates.[38–42] One possible solution could be the physical modeling of the flow behavior which could expand the considered shear rate ranges.[43] Particularly in the high shear rate regions, the viscosity approaches the constant infinity shear viscosity.

As can be seen in Fig. 6, the less expensive carbon paste fits quite well to the cathode catalyst pastes in the mid-shear rate region. Usually, the lower carbon surface area and the absence of Pt particles would exhibit a lower viscosity,[33] but because of the higher volume fraction of Vulcan XC72R carbon (see C/S, Carbon-to-Solvent ratio in Table 1) within the paste, the viscosity is increased to reach similar viscosity regions compared to the cathode catalyst paste. Nevertheless, the infinity shear viscosity indicates that there might be differences between the pastes during printing due to the increased carbon content.

High water content leads to smaller agglomerates of the Pt/C, hence more porosity, which improves O_2-transport[44] and might lead to an increase in viscosity. Moreover, the ionomer interaction / adsorption at the Pt/C surface increases for higher water contents. On the other hand, if the water content is too low, larger, free ionomer aggregates are forming without interacting with the Pt/C-surface.[45]

Therefore, the higher viscosity of the catalyst paste with water could be due to the stronger interactions/adsorption of ionomer to the Pt/C particles, hence creating a stronger resistance against the shear forces. An additional effect could be the higher surface tension of water, which tends to pin at the edges of the parallel plate system and therefore causes additional adhesion forces, which might influence the low shear rate region.

The transition from solid to fluid, the so-called yield stress τ_y, is an important property of pastes for screen printing applications. Already during flooding, the mesh openings are filled with paste only if the yield stress of the paste is locally exceeded.[36] However, if the yield stress is too low, the paste would drip through the openings (if the surface tension is low), which would destabilize the printing process.[46]

Compared to other applications of, e.g., pastes with zinc oxide particles (τ_y = 92–928 Pa)[36] or silver metal pastes (τ_y = 1045–1237 Pa),[19] the yield stress of the carbon paste used in this study is comparably low with $\tau_y \approx 9$ Pa (see Figs. 7, 8) due to the different materials (carbon aggregates, ionomer) compared to, e.g., silver particle mass fraction of 90 ± 5%[19] within the paste.

Flatbed screen printing with carbon suspension

During the screen printing process, four areas are printed within one process step, which is illustrated in Fig. 9. The resulting specific layer weights can be divided in different sections that occur while printing. At first, the dry screen needs to be wetted with paste, leading to a stabilization of the process during the first, e.g., three prints (here defined as section A). These layers are not considered for further investigation. In section B, a stable process is running over several printing steps. Even small changes in the layer weight could later lead to differences in the platinum loading, which has direct influence on the electrochemical

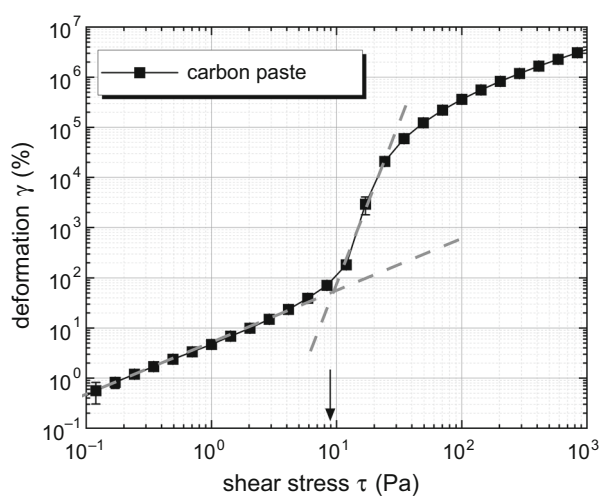

Fig. 7: Deformation of the paste volume by increase in shear stress. The static yield stress can be determined with the tangential method[47] $\tau_y \approx 9$ *Pa* at 70% deformation

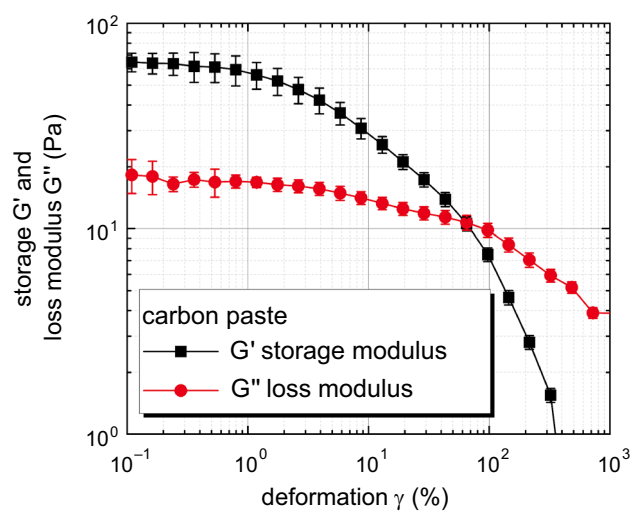

Fig. 8: Strain amplitude sweep during oscillation to measure storage and loss modulus of carbon paste. The intersection G' = G'' marks the transition from solid to fluid flow behavior and is known as dynamic yield stress.[47] (here $\tau_y = 9.77$ *Pa* ± 0.79 *Pa* at ~ 65% deformation)

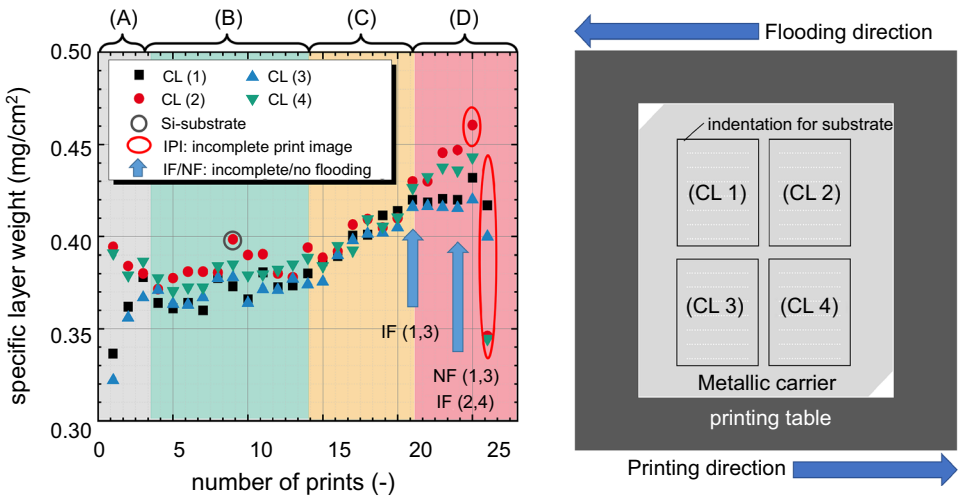

Fig. 9: Left: Example of printing result from group 3: v = 100 mm/s, 50 N, 230/30 mesh. Each printing process can be determined in four sections: (A) Process stabilization, (B) Constant layer weight, (C) Solvent evaporation, (D) Break down due to low paste mass. Right: Schematic representation of the printing table. Within one printing step four layers are coated. It can be noted that catalyst layers (CL) (2) and (4) are flooded at first and show slightly higher layer weights

performance. Therefore, a minimum deviation of cathode Pt-loading is defined $\Delta\omega_{Pt}$= 0.01 mg/cm^2. In terms of the carbon (Pt-free) paste, the layer weight deviation can be transferred by the usual platinum amount within the dry catalyst layer, which gives a maximum allowable layer weight deviation of Δm_{dry} = 0.022 mg/cm^2. This maximum deviation only applies to cathode layer considerations, because anode deviations could be within a wider range, which will verified in the section of electrochemical testing below.

Eventually, the carbon paste is consumed and the ratio between paste volume and paste surface exposed to air surpasses a critical value. During section C, the remaining amount of paste continuously loses its solvent mass, due to the low boiling point (120°C) and high vapor pressure (11.5 hPa) of PGME, until the volume of paste on the screen is too low for a complete flooding of the opening areas, hence the first inhomogeneous structures and incomplete printing images occur (D). Furthermore, the printed areas of CL (2) (red circles) and CL (4) (green triangles) show a slightly higher specific weight over all sections. These phenomena could be explained by the direction of flooding and printing. The amount of paste in front of the flooding bar is larger at the beginning, filling the mesh with a higher paste volume. This effect might be small and therefore negligible if the overall amount of paste on the screen is not critically low. This can be confirmed by the increase of differences between CL (2,4) and CL (1,3) in section (D).

Within the next graphs in Fig. 10, all four simultaneously printed layers are shown as mean with standard deviations. A high standard deviation at the end of the process indicates the complete consumption of the paste and therefore the end of the process. In Fig. 10, the layer weights, corresponding to the process parameter variation of Fig. 3, indicate that the squeegee pressure and velocity have only a minor effect on the printed mass itself. Increasing the squeegee force on the mesh results in a lower paste deposition because the angle between mesh and substrate is reduced, hence the separation of paste from the mesh happens with less shearing forces.[20]

However, the variation of the meshes result in defined changes of the layer weight. Coarse meshes (e.g. 230/30) transfer more paste volume due to the higher mesh thickness and hence higher theoretical volume $V_{th,wet}$ equation (2). The reached number of prints shows that with finer mesh (400/18), less paste volume is applied and therefore the initial volume of paste on the screen lasts longer.

In group 2 the squeegee velocity of 100 mm/s shows the lowest specific layer weight. Potts et al.[18] investigated the paste separation process at different squeegee speeds with a high-speed camera. Directly behind the squeegee (contact point of screen and substrate), the paste sticks to the screen and the substrate simultaneously, which is called "adhesion zone". After that the paste separates as filaments as the mesh moves away from the substrate, which is called "flow to separation". The length of each zone can depend on the printing process parameters. Particularly for low squeegee velocities the zone of flow separation increases in length, hence more filaments are formed at lower speeds. An increase or decrease of printed layer weight is dependent on the rheology of each individual paste. Too low squeegee speeds could lead to a general failure of the printing process with extremely inhomogeneous wet layer thickness and therefore an overall higher layer weight, which could be the case for the 50 mm/s in this study. At 100 mm/s the printed paste mass is lower compared to 300 mm/s which is consistent with the publication of Riemer.[20] By increasing the printing speed, the hydrostatic

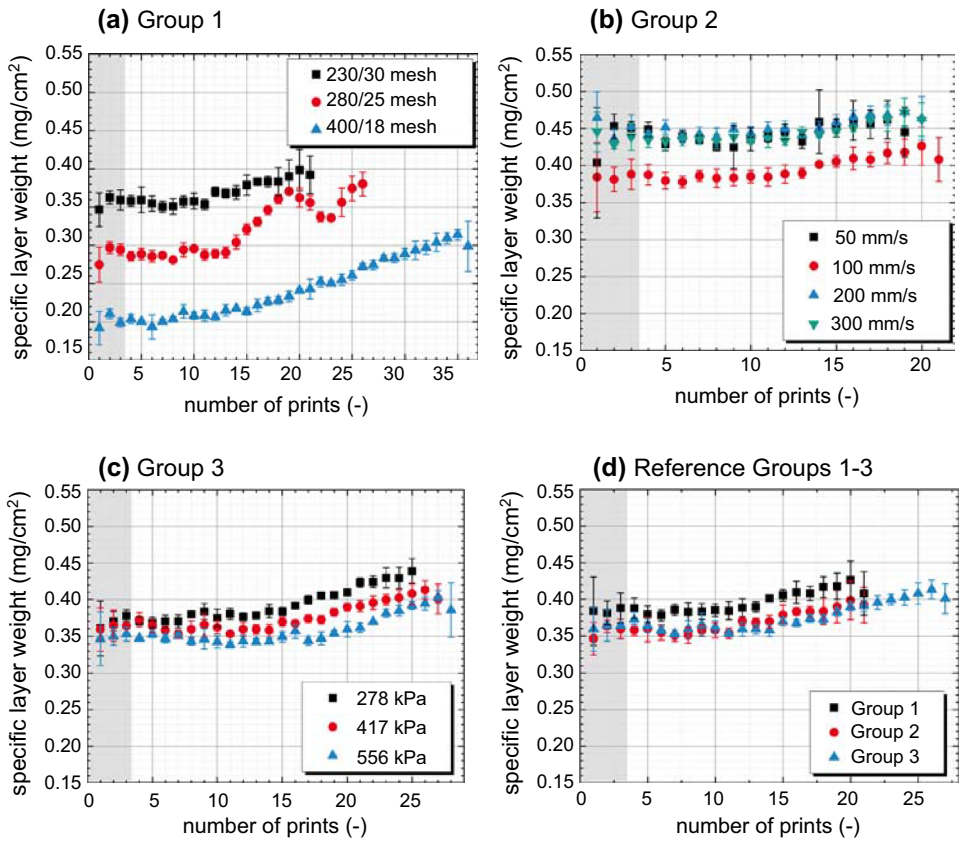

Fig. 10: Top right: variation of printing squeegee velocity, top left: variation of meshes, bottom left: variation of printing squeegee pressure and their impact on the specific layer weight. In each printing step, four catalyst layers have been printed. Bottom right: Reference from each group produced with 230/30 mesh, 417 kPa and 100 mm/s

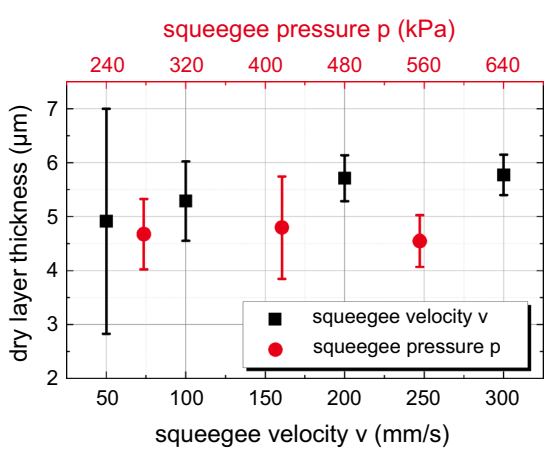

Fig. 11: Squeegee velocity and pressure in dependence on the measured dry layer thickness. With increase of velocity, the process shear rate rises, and the layer surface roughness decreases due to less and smaller agglomerates

pressure within the paste is increased, resulting in higher deposited layer mass.

The measured layer thicknesses from several SEM images are shown in Fig. 11. With increasing velocity, the standard deviation decreases, which reveals a "homogenization" of the coated surface. Figure 12 shows SEM images of the printed layer surface manufactured at different velocities (Group 2). At 50 mm/s slightly more agglomerates and inhomogeneities in thickness (brighter spots) are visible. At higher process shear rates $\dot{\gamma}$ larger agglomerates could break-up within the carbon paste. Additionally, the layer thickness may vary due to instabilities of the printing process. It indicates that further effort should be done to improve the paste dispersion methods prior to the coating process. Nevertheless, more homogeneous layers at higher process speeds could be beneficial for high throughput production.

The error bars of the real paste volume $V_{\mathrm{real,wet}}$ in Fig. 13 are calculated from the measurement errors of

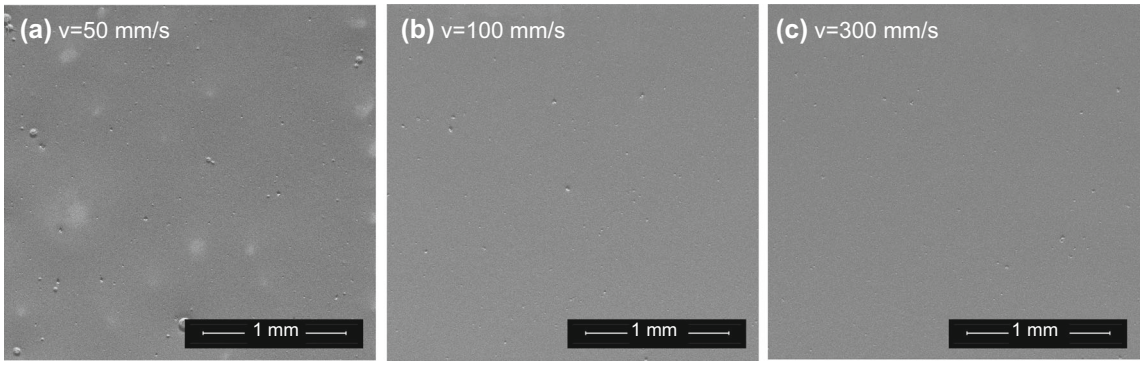

Fig. 12: SEM images of the printed layers manufactured at different squeegee velocities: (a) 50 mm/s, (b) 100 mm/s, (c) 300 mm/s on a silicon substrate (Group 2 samples)

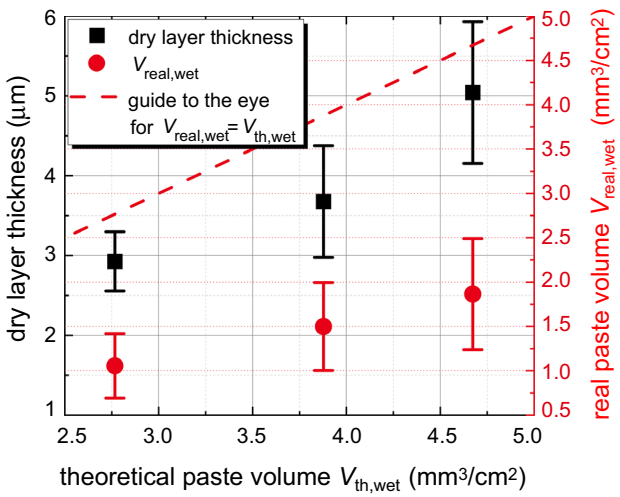

Fig. 13: Based on the mesh type, the theoretical specific volume of paste can be calculated [see equation (2)] and correlated with the measured dry layer thickness (black) or the specific volume calculated by measuring the dry layer weight [see equation (3)]. The guide to the eye shows if $V_{th,wet} = V_{real,wet}$

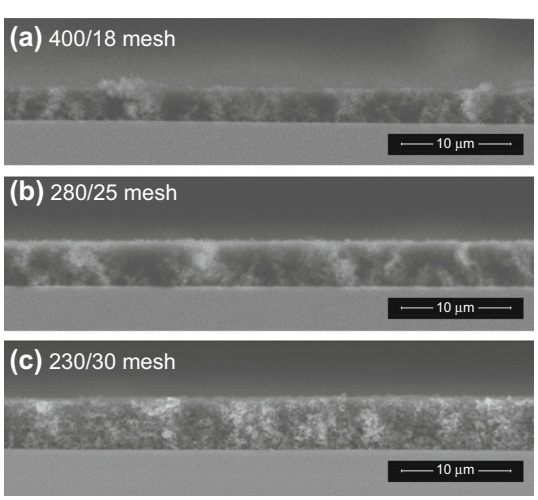

Fig. 14: SEM images of the dry layer cross section by varying the mesh type

the layer mass and their deviations in printing section (B), the deviation of the paste density measurement and an estimated error of ± 5 wt% for the paste solid content due to inevitable evaporation.

To compare mesh types with the measured thickness and specific layer weight, the theoretical volume from Table 2 is used. Figure 13 shows that the calculated theoretical paste volume correlates with the dry layer thickness, which is illustrated in the SEM images of Fig. 14 as well.

However, when comparing the calculated mesh volume $V_{th,wet}$ to the real paste volume $V_{real,wet}$ (red points), the slope verifies the correlation and runs almost parallel to an ideal guide of the eye, which means that the mesh geometry influences the deposited amount of paste. Nevertheless, large amount of paste (60–62%) is not transferred and rather sticking within the wire mesh. In general, the paste separation process is an interplay between the adhesion of the paste on the wire surface, its viscosity and inner forces (cohesion) as well as the adhesion to the substrate. In this case, the substrate is a PTFE-covered glass fiber fabric (decal foil) with very low surface energy of 18–20 mN/m and almost no polar part.[48] However, later in the fabrication process the dry catalyst layer must be separated from the decal foil to the membrane. Therefore, redesigning the surface energy of the substrate, should be done by considering the hot-pressing process. Another way of adhesion optimization could be the choice of solvents within the paste recipe, which might also influence the rheology of the paste. Pastes with lower viscosity and lower yield stress during snap-off might be beneficial for the separation from the wires. On the other hand, lower viscosity often means lower solid content of the paste and therefore a smaller dry layer mass. According to Riemer[20] all parameters that increase the pressure of the paste right in front of the squeegee would lead to a higher paste deposition. Therefore, e.g. the squeegee angle could be decreased.

Additionally, the remaining paste volume in the meshes is slightly different for the meshes. Since all other printing parameters have been kept constant, this

Table 3: Comparison of different meshes for the remaining paste within the mesh and the specific surface area $A_{surf,wire}$

Mesh type	Remaining paste within the mesh $(V_{th,wet} - V_{real,wet})/V_{th,wet}$ (-)	Specific surface area of wire mesh $A_{surf,wire}$(mm^2/cm^2)	Screen tension σ_{max}(N/cm)
230/30	0.6009	176.9	31
280/25	0.6133	179.6	29
400/18	0.6185	185.1	18

The values of screen pretension have been given by the manufacturer.

difference could result from two factors: the surface area of the wires per cm^2 and the lower pretension of a screen σ_{max}. The specific surface area $A_{surf,wire}$ is calculated for each mesh according to equation (4) and shown in Table 3. As can be seen, the surface area of the 400/18 mesh is slightly higher and the screen tension lower compared to the other meshes, therefore more paste sticks to its wires.

Usually, meshes with low wire diameters and comparably low mesh counts are more fragile and sensitive to the applied stress.[27] Therefore, screen manufacturers decrease the pretension in compromise with a longer lifetime of the screen or they change the material from stainless steel to, e.g. tungsten alloys.[27,49] Within this study the wires are made from stainless steel for each mesh, hence the pretension of the 400/18 mesh is lower.

Another phenomenon seen during snap-off is the sticking of the mesh behind the squeegee.[20] When the squeegee moves over the screen, the paste is in contact with the substrate right underneath. The pretension of the screen acts as a force, pulling the screen up to its original position. Nevertheless, a counterforce, which is the drag of the paste that is already in contact with the substrate, could hold the screen down for a certain length behind the squeegee. This length is called the cling zone.[20] This phenomenon leads to an uncontrolled abrupt jump of the screen at which the paste laydown on the substrate could be very low. Additionally, the time delay of the snap-off after the cling zone equals a "resting time" for the paste, which could cause an increase in viscosity and therefore less transferred paste. To avoid a possible cling zone, the snap-off distance should be increased when printing with the 400/18 mesh.

Until this point, only small amounts of paste have been applied on the screen, due to high material costs of Pt/C and ionomer dispersion. However, to proof scalability of the screen printing process, Fig. 15 shows the layer weight for an initial 39.5 g of paste on the screen. For this, 152 layers have been successfully printed and more would have been possible. The solvent evaporation at this scale is not visible, nevertheless existent. Evaporation might remain a problem in industrial production, when "old" paste on the screen is mixed with "fresh" paste to keep the process running.

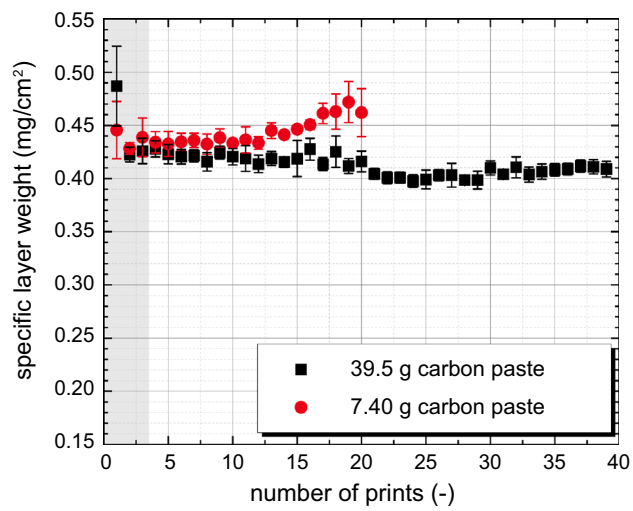

Fig. 15: Increase of the amount of paste on the screen. All other parameters have been kept constant. The printing process of the 39.5 g paste has been stopped by the operator after 38 prints. More prints would have been possible

Flatbed screen printing with catalyst suspension

The Pt-loading has been calculated according to equation (5). The Pt-loading of the catalyst layer increases by choosing coarser meshes, as can be seen in Fig. 16 for both anode pastes. Again, the highest number of prints has been reached with the finest mesh of 400/18, because it results in the lowest layer weight per print.

The cathode paste without water yields at higher Pt-loadings, which might be due to the reduction of the polar part of the surface tension. Since the PTFE substrate has almost no polar bonding part of its surface energy, the wetting behavior of the water-free paste is increased. Therefore, from a process optimization perspective, adjusting the polar and dispersive energy of the pastes through the choice of the solvent mixture, the filament breakup will be affected, changing the deposited layer weight.

The water evaporation can be slightly seen for the cathode CL with water by the increase of Pt-loading. For future experiments it is crucial to select solvents with higher boiling points to enhance the process

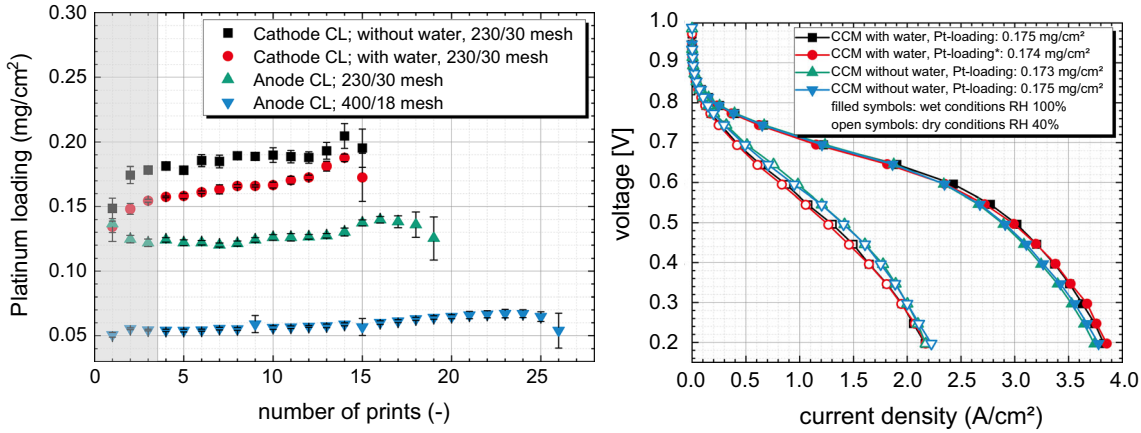

Fig. 16: Left: Platinum loadings with anode and two cathode catalyst pastes: with (15.8 wt%) water and without water. Right: Polarization curve of four CCMs characterized in dry conditions (relative humidity (RH) 40%, open symbols) and wet conditions (RH 100%, filled symbols). Every CCM has an anode loading of 0.055 mg/cm^2, except the red indicated CCM* with 0.12 mg/cm^2 at the anode

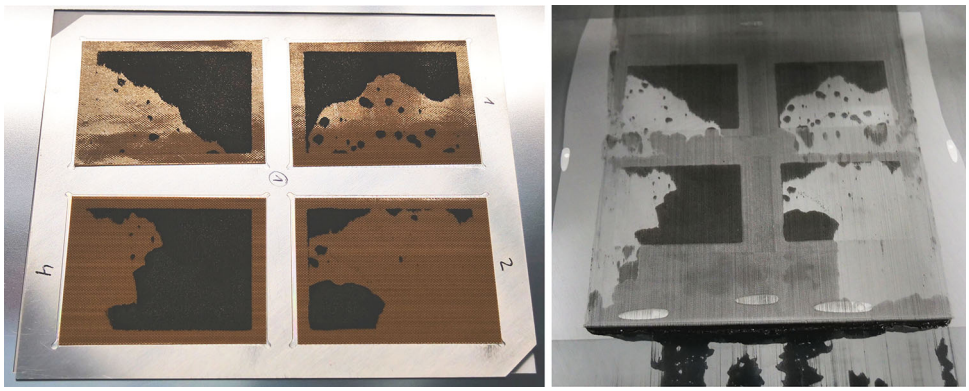

Fig. 17: After second printing step with carbon paste of 100% water content within the liquid part, left: partially printed on PTFE decal foils; right: screen openings with partially filled mesh units of the same paste

stability and reproducibility. This must be done carefully because changing paste recipes will always affect the fuel cell performance while drying temperatures might be limited as well.

Electrochemical characterization

Four CCMs have been tested electrochemically. Two CCMs were made with water on the cathode side and two CCMs without water (within the ink dispersion). The production process of CCMs (catalyst coated membranes) and their performance show a high reproducibility. Two similar CCMs each have been chosen to investigate the deviations during production. Both CCMs made without water have an anode Pt-loading of 0.055 mg/cm^2 and show very good reproducibility. One of the CCMs with water is combined with an anode Pt-loading of 0.12 mg/cm^2 to see if rather large changes of the Pt-loading on the anode side (here $\Delta\omega_{Pt}$= 0.065 mg/cm^2) would influence the performance of the cell. Due to Fig. 16, the change in anode Pt-loading is neglectable, which allows for a larger deviation of layer weight during the coating process at least for anode catalyst layers. The electrochemical surface area (ECSA) of the CCMs has been measured as: 65.11 ± 0.62 cm^2/cm^2 (CCMs with water) and 64.34 ± 2.07 cm^2/cm^2 (CCMs without water), which is in agreement with our previous study.[8]

As can be seen in Fig. 16, the performance of the catalyst layers produced with and without water differs significantly, depending on the relative humidity during electrochemical testing. At RH = 100% the CCMs with water show higher current densities mainly in the diffusion region. Recent studies of van Cleve et al.[44,45] claim that there might be an optimum water content within the catalyst paste. At lower water content, the ionomer particles tend to agglomerate with low interaction of ionomer to the Pt/C particle surface, hence the adsorbed ionomer film might be too thin or in some

parts not even attached to the catalyst. Therefore, the addition of slightly more water could already enhance the interaction of ionomer and Pt/C. The direct influence of the relative humidity during in-situ testing has not yet been investigated systematically. Therefore, the optimum water content might shift in dependence of the electrochemical testing conditions.

However, from a coating process perspective, higher water contents will not only lead to evaporation issues, but also to wetting problems on the decal foil, which can be seen in Fig. 17. Due to the high contact angle of water on PTFE substrates, the adhesion on the PTFE substrate is lower, hence a greater amount of paste sticks within the mesh and is not separated properly. Additionally, the high surface tension might be the reason why the paste is not spread over the screen during flooding in the first place. In general, screen printing technology is strongly influenced by the interactions of adhesion and cohesion forces from mesh to paste, paste itself and paste to substrate.

Therefore, changing the paste recipe for the purpose of process optimization must be carried out taking into consideration its effect on the fuel cell performance.

Another possible solution might be the integration of a dispensing unit in front of the squeegee. Hence, further experiments considering different solvents are currently being conducted and will follow within the scope of this study.

Conclusions

Screen printing process parameters like printing velocity, squeegee pressure and different meshes have been varied to evaluate their impact on the specific layer weight and thickness of catalyst layers for PEM fuel cells. It was shown that the adjustment of the Pt-loading should be done by changing the mesh, whereas the increase of the printing speed results in a more homogeneous coating thickness. Both results were verified by SEM images. The calculation of the theoretical paste volume within the mesh has been extended to account for the calendared mesh thickness. Nevertheless, 60–62% of the paste stick to the mesh during the filament separation. Therefore, further optimization of the snap-off process is necessary.

Two different catalyst pastes with and without water have been printed and electrochemically tested, as well as analyzed by viscosity measurements. Catalyst pastes without water content show a decrease in dynamic viscosity and applied Pt-loading as well as performed best at dry conditions (+ 66 $mW/cm^2 \pm 32 mW/cm^2$ at 0.6 V), compared to fabrication of catalyst layers with water. However, at wet conditions the catalyst layers without water showed a lower power density in the diffusion region (− 48 $mW/cm^2 \pm 12 mW/cm^2$ at 0.4 V).

Additionally, it has been shown that scaling the fabrication of catalyst layers with constant process parameters is highly reproducible and exhibits very good overall performance. The main challenge for the screen printing technology is the dependence of process stability on the evaporation of the solvents during the printing process, which causes an increase in Platinum-loading over time. Further studies are currently being conducted to examine air-stable solvents and their effect on fuel cell performance to enable the industrial fabrication of catalyst layers by flatbed or rotary screen printing, flexographic or gravure printing.

Acknowledgments The authors thank the Ministry of the Environment, Climate, Protection and the Energy Sector Baden-Württemberg for the financial support of the project HyFab-Baden-Württemberg, contract no. L7520113 and the Project Agency Karlsruhe, Baden-Württemberg Programs (PTKA-BWP) for the administration as well as both for the good cooperation.

Funding Open Access funding enabled and organized by Projekt DEAL.

Open Access This article is licensed under a Creative Commons Attribution 4.0 International License, which permits use, sharing, adaptation, distribution and reproduction in any medium or format, as long as you give appropriate credit to the original author(s) and the source, provide a link to the Creative Commons licence, and indicate if changes were made. The images or other third party material in this article are included in the article's Creative Commons licence, unless indicated otherwise in a credit line to the material. If material is not included in the article's Creative Commons licence and your intended use is not permitted by statutory regulation or exceeds the permitted use, you will need to obtain permission directly from the copyright holder. To view a copy of this licence, visit http://creativecommons.org/licenses/by/4.0/.

References

1. Kampker, A, Ayvaz, P, Schön, C, Karstedt, J, Förstmann, R, Welker, F, "Challenges Towards Large-Scale Fuel Cell Production: Results of an Expert Assessment Study." *Int. J. Hydrogen Energy*, **45** 29288 (2020)
2. Ulsh, M, Sopori, B, Aieta, NV, Bender, G, "Challenges to High-Volume Production of Fuel Cell Materials: Quality Control." *ECS Trans.*, **50** (2) 919–926 (2013)
3. Wang, W, Chen, S, Li, J, Wang, W, "Fabrication of Catalyst Coated Membrane with Screen Printing Method in a Proton Exchange Membrane Fuel Cell." *Int. J. Hydrogen Energy*, **40** (13) 4649–4658 (2015)
4. Andrade, AB, Bejarano, MLM, Cunha, EF, Robalinho, E, Linardi, M, "Fabrication of High Precision PEMFC Membrane Electrode Assemblies by Sieve Printing Method." *J.*

Fuel. Cell Sci Technol, **6** 2. https://doi.org/10.1115/1.3080556 (2009)
5. Mauger, SA, Neyerlin, KC, Yang-Neyerlin, AC, More, KL, Ulsh, M, ''Gravure Coating for Roll-to-Roll Manufacturing of Proton-Exchange-Membrane Fuel Cell Catalyst Layers.'' *J. Electrochem. Soc.*, **165** (11) F1012–F1018 (2018)
6. Hwang, DS, Park, CH, Yi, SC, Lee, YM, ''Optimal Catalyst Layer Structure of Polymer Electrolyte Membrane Fuel Cell.'' *Int. J. Hydrogen Energy*, **36** (16) 9876–9885 (2011)
7. Santangelo, P, Cannio, M, Romagnoli, M, ''Review of Catalyst-deposition Techniques for PEMFC Electrodes.'' *TI-IJES*, **63** (1) 65–72 (2019)
8. Alink, R, Singh, R, Schneider, P, Christmann, K, Schall, J, Keding, R, Zamel, N, ''Full Parametric Study of the Influence of Ionomer Content, Catalyst Loading and Catalyst Type on Oxygen and Ion Transport in PEM Fuel Cell Catalyst Layers.'' *Molecules (Basel, Switzerland)*, **25** (7) 1523 (2020)
9. Lee, E, Kim, D-H, Pak, C, ''Effects of Cathode Catalyst Layer Fabrication Parameters on the Performance of High-Temperature Polymer Electrolyte Membrane Fuel Cells.'' *Appl Surf Sci*, **510** 145461 (2020)
10. Bladergroen, B, Su, H, Pasupathi, S, Linkov, V, ''Overview of Membrane Electrode Assembly Preparation Methods for Solid Polymer Electrolyte Electrolyzer.'' In: Kleperis, J (ed.) *Voltammetric Characterization Methods for the PEM Evaluation of Catalysts*. INTECH Open Access Publisher (2012)
11. Waldrop, K, Wycisk, R, Pintauro, PN, ''Application of Electrospinning for the Fabrication of Proton-Exchange Membrane Fuel Cell Electrodes.'' *Curr. Opin. Electrochem.*, **21** 257–264 (2020)
12. Brodt, M, Han, T, Dale, N, Niangar, E, Wycisk, R, Pintauro, P, ''Fabrication, In-Situ Performance, and Durability of Nanofiber Fuel Cell Electrodes.'' *J. Electrochem. Soc.*, **162** (1) F84–F91 (2015)
13. Brodt, M, Wycisk, R, Pintauro, PN, ''Nanofiber Electrodes with Low Platinum Loading for High Power Hydrogen/Air PEM Fuel Cells.'' *J. Electrochem. Soc.*, **160** (8) F744–F749 (2013)
14. Shukla, S, Stanier, D, Saha, MS, Stumper, J, Secanell, M, ''Analysis of Inkjet Printed PEFC Electrodes with Varying Platinum Loading.'' *J. Electrochem. Soc.*, **163** (7) F677–F687 (2016)
15. Park, K, Ohnishi, T, Goto, M, So, M, Takenaka, S, Tsuge, Y, Inoue, G, ''Improvement of Cell Performance in Catalyst Layers with Silica-Coated Pt/Carbon Catalysts For Polymer Electrolyte Fuel Cells.'' *Int. J. Hydrogen Energy*, **45** (3) 1867–1877 (2020)
16. Park, I-S, Li, W, Manthiram, A, ''Fabrication of Catalyst-Coated Membrane-Electrode Assemblies by Doctor Blade Method and their Performance in Fuel Cells.'' *J. Power Sour.*, **195** (20) 7078–7082 (2010)
17. Hoffmann, E, Zhang, S, Thoma, M, Damm, C, Peukert, W, ''Formulation of Carbon Black-Ionomer Dispersions for Thin Film Formation in Fuel Cells.'' *Particuology*, **44** 7–21 (2019)
18. Potts, S-J, Phillips, C, Jewell, E, Clifford, B, Lau, YC, Claypole, T, ''High-Speed Imaging the Effect of Snap-Off Distance and Squeegee Speed on the Ink Transfer Mechanism of Screen-Printed Carbon Pastes.'' *J. Coat. Technol. Res.*, **17** (2) 447–459 (2020)
19. Tepner, S, Wengenmeyr, N, Ney, L, Linse, M, Pospischil, M, Clement, F, ''Improving Wall Slip Behavior of Silver Pastes on Screen Emulsions for Fine Line Screen Printing.'' *Solar Energy Mater. Solar Cells*, **200** 109969 (2019)
20. Riemer, DE, ''The Theoretical Fundamentals of the Screen Printing Process.'' *Microelectron. Int.*, **6** (1) 8–17 (1989)
21. Hahne, P, *Innovative Drucktechnologien Siebdruck-Tampondruck*. Verlag der Siebdruck (2001)
22. Pan, J, Quintero, A, Tonkay, GL, ''Screen Printing Process Design of Expmeriments for Fine Line Printing of Thick Film Ceramic Substrates.'' *J. Electron. Manuf.*, **09** (03) 203–213 (1999)
23. Scheer, HG, *Siebdruck-Handbuch*. Verlag der Siebdruck (1999)
24. Bonifácio, RN, Paschoal, JOA, Linardi, M, Cuenca, R, ''Catalyst Layer Optimization by Surface Tension Control During Ink Formulation of Membrane Electrode Assemblies in Proton Exchange Membrane Fuel Cell.'' *J. Power Sourc.*, **196** (10) 4680–4685 (2011)
25. Yüce, C, Willenbacher, N, ''Challenges in Rheological Characterization of Highly Concentrated Suspensions – A Case Study for Screen-Printing Silver Pastes.'' *J. Visualized Exper.: JoVE*, **122** 84 (2017)
26. Mehrazi, S, Sarker, M, Mojica, F, Rolfe, P, Chuang, P-YA, ''A Rheological Approach to Studying Process-induced Structural Evolution of the Microporous Layer in a Proton Exchange Membrane Fuel Cell.'' *Electrochimica Acta*, **389** 138690 (2021)
27. Ney, L, Tepner, S, Linse, M, Lorenz, A, Bechmann, S, Weber, R, Pospischil, M, Clement, F, ''Optimization of Fine Line Screen Printing Using In-depth Screen Mesh Analysis.'' AIP Conference Proceedings, 20006 (2019)
28. Horvath, E, Harsanyi, G, ''Mechanical Modelling and Life Cycle Optimisation of Screen Printing.'' *J. Theor. Appl. Mech.*, **50** 1025–1036 (2012)
29. Li, T, Shen, J, Chen, G, Guo, S, Xie, G, ''Performance Comparison of Proton Exchange Membrane Fuel Cells with Nafion and Aquivion Perfluorosulfonic Acids with Different Equivalent Weights as the Electrode Binders.'' *ACS Omega*, **5** 17628 (2020)
30. Ghielmi, A, Vaccarono, P, Troglia, C, Arcella, V, ''Proton Exchange Membranes Based on the Short-Side-Chain Perfluorinated Ionomer.'' *J. Power Sourc.*, **145** (2) 108–115 (2005)
31. Aoki, Y, Hatano, A, Watanabe, H, ''Rheology of Carbon Black Suspensions. I. Three Types Of Viscoelastic Behavior.'' *Rheol. Acta*, **42** (3) 209–216 (2003)
32. Barrie, CL, Griffiths, PC, Abbott, RJ, Grillo, I, Kudryashov, E, Smyth, C, ''Rheology of Aqueous Carbon Black Dispersions.'' *J. Colloid Interface Sci.*, **272** (1) 210–217 (2004)
33. Khandavalli, S, Park, JH, Kariuki, NN, Myers, DJ, Stickel, JJ, Hurst, K, Neyerlin, KC, Ulsh, M, Mauger, SA, ''Rheological Investigation on the Microstructure of Fuel Cell Catalyst Inks.'' *ACS Appl. Mater. Interfaces*, **10** (50) 43610–43622 (2018)
34. Lu, S, Chung, D, ''Viscoelastic Behavior of Carbon Black and its Relationship with the Aggregate Size.'' *Carbon*, **60** 346–355 (2013)
35. O'Mahony, C, Haq, EU, Sillien, C, Tofail, SAM, ''Rheological Issues in Carbon-Based Inks for Additive Manufacturing.'' *Micromachines*, **10** (2) 99 (2019)
36. Xu, C, Willenbacher, N, ''How Rheological Properties Affect Fine-Line Screen Printing of Pastes: A Combined Rheological and High-Speed Video Imaging Study.'' *J. Coat. Technol. Res.*, **15** (6) 1401–1412 (2018)
37. Tepner, S, Wengenmeyr, N, Linse, M, Lorenz, A, Pospischil, M, Clement, F, ''The Link Between Ag-Paste Rheology and Screen-Printed Solar Cell Metallization.'' *Adv. Mater. Technol.*, **5** 2000654 (2020)

38. Hemingway, EJ, Kusumaatmaja, H, Fielding, SM, ''Edge Fracture in Complex Fluids.'' *Phys. Rev. Lett.*, **119** (2) 28006 (2017)
39. Keentok, M, Xue, S-C, ''Edge Fracture in Cone-Plate and Parallel Plate Flows.'' *Rheol. Acta*, **38** (4) 321–348 (1999)
40. Mattes, KM, Vogt, R, Friedrich, C, ''Analysis of the Edge Fracture Process in Oscillation for Polystyrene Melts.'' *Rheol. Acta*, **47** (8) 929–942 (2008)
41. Tanner, RI, Keentok, M, ''Shear Fracture in Cone-Plate Rheometry.'' *J. Rheol.*, **27** (1) 47–57 (1983)
42. Zarraga, IE, Hill, DA, Leighton, DT, ''Normal Stresses and Free Surface Deformation in Concentrated Suspensions of Noncolloidal Spheres in a Viscoelastic Fluid.'' *J. Rheol.*, **45** (5) 1065–1084 (2001)
43. Ney, L, Singh, R, Göttlicher, N, Le Hoang-Phuong, Tepner, S, Klingele, M, Keding, R, Clement, F, ''Modeling the Flow Behavior of Catalyst Inks for PEM Fuel Cells by an Evolutionary Algorithm.'' (2021)
44. van Cleve, T, Wang, G, Mooney, M, Cetinbas, CF, Kariuki, N, Park, J, Farghaly, A, Myers, D, Neyerlin, KC, ''Tailoring Electrode Microstructure via Ink Content to Enable Improved Rated Power Performance for Platinum Cobalt/High Surface Area Carbon Based Polymer Electrolyte Fuel Cells.'' *J. Power Sources*, **482** 228889 (2021)
45. van Cleve, T, Khandavalli, S, Chowdhury, A, Medina, S, Pylypenko, S, Wang, M, More, KL, Kariuki, N, Myers, DJ, Weber, AZ, Mauger, SA, Ulsh, M, Neyerlin, KC, ''Dictating Pt-Based Electrocatalyst Performance in Polymer Electrolyte Fuel Cells, from Formulation to Application.'' *ACS Appl. Mater. Interfaces*, **11** (50) 46953–46964 (2019)
46. Trease, RE, Dietz, R, ''Paste Rheology Can Improve Your Fine Line Printing.'' Proceedings ISHM, p.8.4.2 (1970)
47. Mezger, TG, *The Rheology Handbook*. Vincentz Network (2012)
48. Szymczyk, K, Jańczuk, B, ''Surface Tension of Polytetrafluoroethylene and Polymethyl Methacrylate Under the Influence of the Fluorocarbon Surfactant Film.'' *Ind. Eng. Chem. Res.*, **51** (43) 14076–14083 (2012)
49. Tepner, S, Ney, L, Linse, M, Lorenz, A, Pospischil, M, Clement, F, ''Studying Knotless Screen Patterns for Fine-line Screen Printing of Si-Solar Cells.'' *IEEE J. Photovolt.*, **10** (2) 319–325 (2020)

Publisher's Note Springer Nature remains neutral with regard to jurisdictional claims in published maps and institutional affiliations.